Microscopic Imaging Through a Turbid Medium by Use of a Differential Optical Kerr Gate

Yuhu Ren, Jinhai Si, Wenjiang Tan, Shichao Xu, Junyi Tong, and Xun Hou

Abstract—Microscopic imaging of hidden objects in scattering media is demonstrated using a differential optical Kerr gate (DOKG). The results show that the high spatial frequency components of the imaged object filtered by the optical Kerr gate can be considerably compensated using the DOKG. Microscopic images with a maximal lateral resolution of ∼2-μm can be achieved. Compared with OKG microscopic imaging, the contrast of DOKG microscopic images is enhanced significantly.

Index Terms—Microscopy, Kerr effect, turbid media, ultrafast optics.

I. INTRODUCTION

OPTICAL imaging of hidden objects in highly scattering media is important in many areas such as in clouds [1], fogs [2], or aerated sprays [3]. When light pulses propagate through a turbid medium, the transmitted pulses consist of a ballistic component, a snake component, and a diffuse component [4]. The ballistic photons that carry the object information migrate through a turbid medium undeviated in the forward direction and arrive first. The snake component consists of the photons that have undergone only a few scatterings along quasi-straight-line paths. The diffuse component that has been scattered randomly in all directions loses the image information and constitutes the noise [5]. The image quality is often degraded by multiple scattering in a scattering medium, which presents the main challenge associated with optical imaging [6]. Many different techniques have been introduced to image or probe objects embedded in scattering media [7]–[10]. A feasible way to suppress multiple scattered photons and improve the visualization of objects hidden in the turbid medium is by employing a short time gate based on nonlinear optical phenomena, such as degenerate four

Y. Ren, J. Si, W. Tan, S. Xu, and X. Hou are with the Key Laboratory for Physical Electronics and Devices and the Shaanxi Key Laboratory of Information Photonic Technique, Collaborative Innovation Center of Suzhou Nano Science and Technology, School of Electronics and information Engineering, Ministry of Education, Xi'an Jiaotong University, Xi'an 710049, China (e-mail: renyuhuh@sina.com; jinhaisi@mail.xjtu.edu.cn; tanwenjiang@mail.xjtu.edu.cn; xusc1011@sina.com; 332515787@qq.com).

J. Tong is with the Department of Applied Physics, Xi'an University of Technology, Xi'an 710048, China (e-mail: 85951917@qq.com).

wave mixing [11], second-harmonic generation [12], or an optical Kerr gate (OKG) [13], [14]. Among the available time gating techniques, OKG imaging has been investigated widely due to its advantages, such as no need for satisfying the phase matching condition or the high intensity of the imaging signal [15]. However, most studies on OKG imaging focus on the macroscopic imaging of hidden objects in a scattering medium.

Microscopy has been a critical technology for examining small features in many physical, chemical, and biological systems [16], [17]. Notable examples of microscopy imaging such as optical coherence microscopy [18], focal modulation microscopy [19] and confocal microscopy [20] have been used to obtain clear images of objects hidden in or behind highly scattering turbid media. However, most of the microscopy techniques mentioned above are scanning imaging methods and limited to image the slow-moving objects such as human eye imaging in vivo [18], and even the stationary objects. On the contrary, OKG imaging can provide an effective approach to obtain the image of high-speed mobile object hidden in highly scattering turbid media. For instance, OKG imaging can resolve clean images of the structures in the high pressure and dense spray region, which rapidly change on the time scale of a few microseconds [21]. Therefore, the combination of optical microscopy and ultrafast OKG stands to enable technology in obtaining microscopic OKG imaging in turbid media. However, in microscopic OKG imaging the gating pulse can induce a transient spatial aperture in the Kerr material in the OKG, which filters the high spatial frequencies components of the detected object [22]. Therefore, the spatial resolution of the imaging system decreases.

In this letter, we demonstrate a new method for microscopic imaging through a turbid medium by use of a differential optical Kerr gate (DOKG). A sequence of microscopic images of a test chart hidden behind a highly scattering medium was obtained by using the ultrafast DOKG technique. Compared with OKG microscopic imaging, the contrast of microscopic images obtained by using the DOKG technique is enhanced significantly. In addition, the experimental results show that a maximum lateral resolution of approximately 2 μm of the DOKG microscopic imaging in a turbid medium can be achieved.

II. EXPERIMENTAL SETUP

The schematic of the differential optical Kerr gate microscopy imaging system is shown in Fig. 1(a). A Ti: sapphire laser produced 800 nm, 50 fs pulses at a repetition
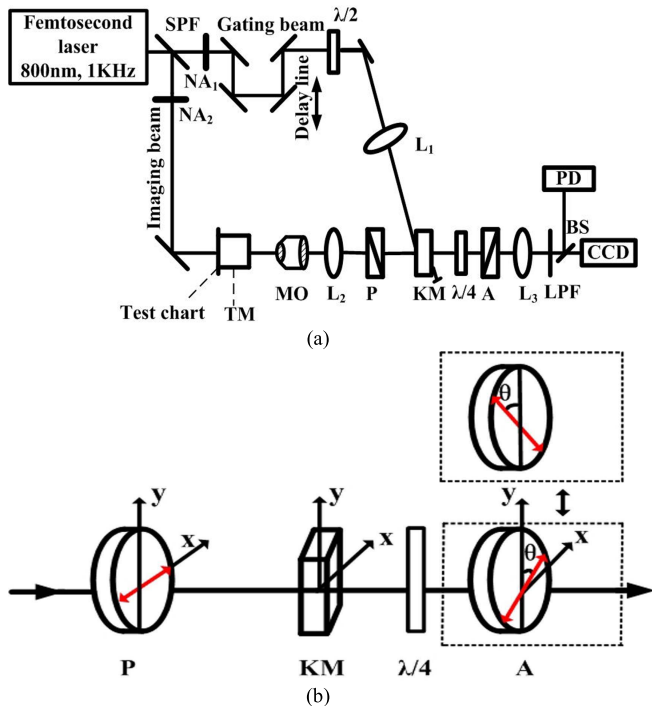
(a)

(b)

Fig. 1. (a) Experimental setup for the DOKG microscopy imaging system. (b) Schematic of the DOKG. SPF: short pass filter; $\lambda/2$: half-wave plate; $\lambda/4$: quarter-wave plate; P: polarizer; A: analyzer; NA: neutral attenuator; LPF: long pass filter; TM: turbid media; KM: Kerr medium; BS: beam splitter; MO: microscope objective; θ: the angle between the polarization direction of the analyzer and the vertical direction. L: lens (the focal lengths of lenses L_1, L_2, L_3 were 160 mm, 100 mm, and 150mm, respectively).

rate of 1 kHz. The full width at half maximum (FWHM) of the laser spectrum was about 30 nm. The laser beam was split into a gating beam centered at 780 nm and an imaging beam centered at 800 nm by a short pass filter (SPF). The intensity of the gating beam and the imaging beam were adjusted by neutral attenuators (NA$_1$ and NA$_2$, respectively). The power of the gating beam and the imaging beam were 0.58 W and 0.40 W, respectively. The imaging beam was first modulated by a 1.41-line-pair/mm resolution chart (a chromium-coated glass U.S. Air Force resolution chart) and then introduced to a turbid medium. The transmitted light from the turbid medium was introduced into the microscope objective [10×numerical aperture (NA) = 0.25, Nikon]. The transmitted light was first focused by lens (L$_2$) and then introduced into the DOKG. The polarization of the gating beam was first linearly polarized at 45° with respect to the polarization of the imaging beam for optimal efficiency using a half-wave ($\lambda/2$) plate. Thereafter, the gating beam was focused into the Kerr medium of CS$_2$ filled in a 5 mm quartz cell to the ultrafast OKG imaging in the turbid medium. A long pass filter (LPF) was placed before the beam splitter (BS) to block light noise caused by the gating beam scattered forward into the detecting devices.

In this setup, the imaging pulse was spatially overlapped with the gating pulse in the Kerr medium which was placed at the focal plane of a compound lens consisting of the microscope object and lens (L$_2$). When the two pulses were spatially and temporally overlapped, the imaging pulse polarization was
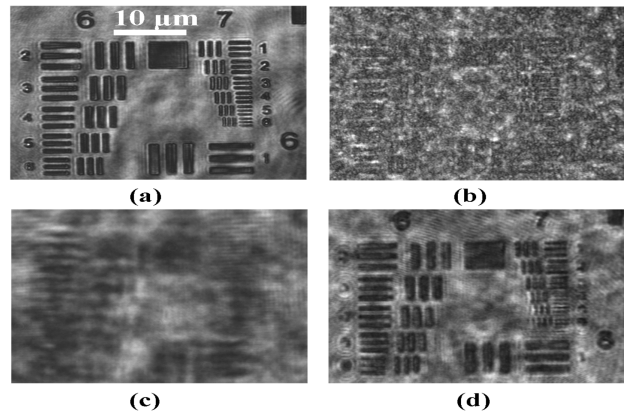

Fig. 2. Images of the test chart behind water and the polystyrene microsphere turbid medium. (a) Reference image. (b) No time gate (standard transillumination). (c) OKG image for the polystyrene microsphere turbid medium. (d) DOKG image for the polystyrene microsphere turbid medium.

rotated due to the birefringence of the Kerr media induced by the gating pulse. Then part of the imaging pulse passed through the analyzer. Due to the time-gated nature of the experiment, the imaging pulse was synchronously detected by a charge coupled device (CCD) camera and a photodiode (PD).

As shown in Fig. 1(b), the DOKG consisted of a polarizer, a Kerr medium, a quarter-wave plate ($\lambda/4$), and an analyzer. In the DOKG, the polarizer was set parallel to the x direction. The quarter-wave plate ($\lambda/4$), with its optical axis parallel to the polarizer, was placed between the Kerr medium and the analyzer to provide a $\pi/2$ optical phase bias [23]. The angle between the polarization direction of the analyzer and the vertical direction is denoted as heterodyne θ. By placing a quarter-wave plate before the analyzer and rotating the analyzer by a few degrees, the DOKG imaging can be implemented. This is different from a standard OKG, in which the polarization direction of the polarizer is horizontal (x direction), the polarization direction of the analyzer is vertical, and no optical phase bias is provided. DOKG images are acquired by subtracting image I from image II, in which image I and image II are obtained at angles of θ and $-\theta$, respectively. Here, the angle θ is set at 8°.

The turbid medium was composed of a polystyrene microsphere solution contained in a cubic cuvette with inside dimensions of 50 mm × 50 mm × 10 mm. The thickness of the cuvette along the optical axis was 10 mm. The diameter of the polystyrene microspheres was 3.13 μm. The refractive indices of the background medium n_b and the polystyrene microspheres n_p were 1.33 and 1.58, respectively. The absorption of the turbid medium was low enough to be ignored. The value of the optical density of the sample was OD = 10.0.

III. RESULTS AND DISCUSSION

The images of the test chart (a U.S. Air Force 1951 resolution chart) hidden behind a polystyrene microsphere sample are demonstrated by use of DOKG microscopic imaging. In Fig.2 (a), we show direct microscopic imaging for the sample filled with deionized water as the reference image. The direct microscopic image is measured by setting

the two polarizers of the Kerr gate setup parallel to each other, without gate light irradiation. In Fig. 2(b), we show direct microscopic imaging for the sample filled with the polystyrene microsphere turbid medium. The object hidden behind such a turbid medium cannot be seen because the total intensity of the scattered photons is greater than the intensity of the ballistic photons. In Figs. 2(c) and 2(d), we show OKG microscopic imaging and DOKG microscopic imaging, respectively, for the polystyrene microsphere turbid medium. As shown in Fig. 2(c), the boundaries of the shadowed and unshadowed regions for OKG microscopic imaging are highly blurred although it provides improvement in the contrast of the image. From Fig.2 (d), we can see that DOKG microscopic imaging improves image resolution and enhances the contrast between the target and its background. The blur of the boundaries of the shadowed and unshadowed regions for OKG imaging could be attributed to the transient soft aperture in the Kerr material [22], which arises from the finite spot size of the gating beam. The transient soft aperture acts as a low-pass filter, which enables the low spatial frequency components of the imaged object pass but removes the high spatial frequency components. The low spatial frequency components are at the center of the Fourier plane of the compound lens consisting of the microscope object and lens (L$_2$), while the high spatial frequency components are in the peripheral area of the Fourier plane. The high spatial frequency components of the imaged object filtered by the transient soft aperture can be compensated by use of the DOKG.

The difference between the OKG and DOKG imaging can be explained as follows. For the DOKG microscopic imaging, the imaging signal field contains an additional component called local oscillator field $E_{LO}(\theta)$, which arises from the rotation of the polarizer by an angle θ. The local oscillator field compensates the high spatial frequency components of the imaged object. The local oscillator field contains both the low spatial and high spatial frequencies of the imaged object. The detected image intensity for DOKG is $4E_{LO}(\theta)E_{OKG}(t)$, where the term $E_{OKG}(t)$ is the OKG signal field. The detected image intensity is obtained by subtracting the intensity of image I from the intensity of image II, in which the two image intensities are $I_{LO}(\theta) + I_{OKG}(t) - 2E_{LO}(\theta)E_{OKG}(t)$ and $I_{LO}(\theta) + I_{OKG}(t) + 2E_{LO}(\theta)E_{OKG}(t)$, respectively [24]. The image I and image II are obtained at angles of θ and $-\theta$, respectively. Where, the term $I_{LO}(\theta)$ is the intensity of the local oscillator field, and the term $I_{OKG}(t)$ is the intensity of the OKG signal field. Overall, the high spatial frequencies components of the imaged object can be compensated due to the local oscillator field. As a result, the DOKG microscopic imaging is more visible compared with OKG microscopic imaging as shown in Fig. 2. It should be noted that the quarter-wave plate ($\lambda/4$) in our experiment provides a $\pi/2$ out of phase with the rest of the imaging beam to the local oscillator field, which enhances the intensity of the detected signal for the DOKG imaging [23], [25].

To further quantitatively evaluate the performance of OKG and DOKG microscopic imaging systems, we measured the modulation transfer function (MTF) of both systems. The MTF is given by $MTF(f) = C(f)/C_0(f)$, where the image
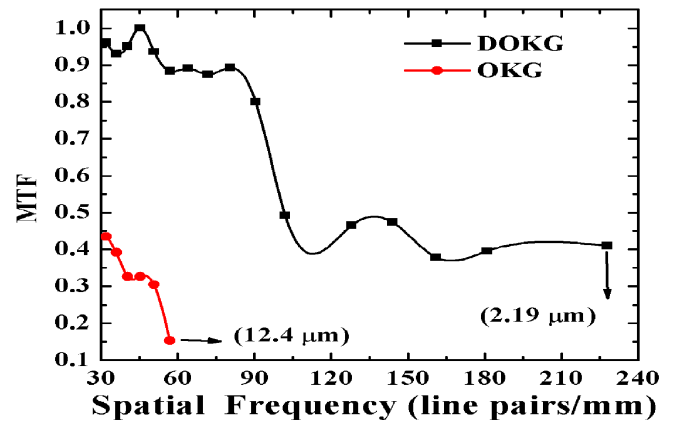

Fig. 3. Comparison of the MTF of the OKG microscopic imaging system and the DOKG microscopic imaging system.

contrast is defined as $C(f) = (I_{max} - I_{min})/(I_{max} + I_{min})$. Further, C_0 (f) denotes the modulation of the object, and f is the spatial frequency. The image contrast is calculated using the average light intensity retrieved from the dark region (I_{min}) and the average light retrieved from the unshadowed region (I_{max}) of the test chart. From Fig.3, we can see that the spatial resolution of the DOKG microscopic images is higher than that of the OKG microscopic images. For DOKG microscopic imaging, the maximum resolvable spatial frequency is 228 line pairs per millimeter (lp/mm), and the corresponding resolved object size is approximately $1mm/(228 \times 2) = 2.19 \mu m$ in our experiments. However, for the OKG microscopic imaging system the maximum resolvable spatial frequency is 40.3 lp/mm, and the corresponding resolved object size is approximately 12.4 μm. From Fig.3, It can also be seen that the contrasts of DOKG images are higher than that of OKG images. The results show that DOKG microscopic imaging could compensate the high spatial frequency components of the object; thus, providing a higher resolvable spatial frequency and a higher contrast.

It should be noted that for DOKG microscopic imaging, the image spatial resolution is dependent on the numerical aperture (NA) of the microscope objective. To obtain high resolution a high numerical aperture objective should be employed. However, the working-distance of the DOKG microscopic imaging system decreases with the increase of the NA of the microscope objective. For example, for the 10× microscope objective with a numerical aperture of NA = 0.25, the working-distance for the DOKG microscopic imaging system is 13 mm, whereas for the 20× microscope objective with a numerical aperture of NA = 0.40, the working-distance for the DOKG microscopic imaging system is only 5 mm. Therefore, a trade-off exists between image spatial resolution and the working-distance of the DOKG microscopic imaging system.

As one of the potential applications, we finally performed an experiment to image an inhomogeneous test chart hidden behind a turbid medium using a DOKG. The inhomogeneous test chart consists of two parts (A and B) of different thicknesses. Part B of the test chart is thicker than part A.
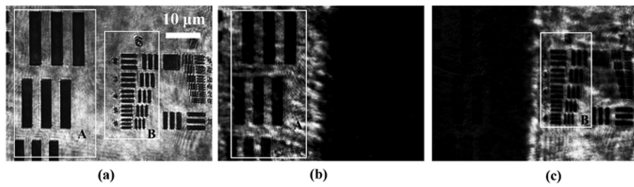
Fig. 4. Images of the inhomogeneous test chart behind water and the polystyrene microsphere turbid medium. (a) No time gate (standard transillumination); images using a DOKG at delay times of (b) 0 ps and (c) 2ps.

In Fig.4 (a), a standard transillumination (not time-gated) image of the inhomogeneous test chart is shown. The time-resolved images of the inhomogeneous test chart are shown in Figs.4 (b) and 4(c). The time $t = 0$ ps is defined to be the time when the light pulse peak passes through part A of the inhomogeneous test chart. In Fig.4 (b), we show the image of the test chart at the time $t = 0$ ps. Part A is resolved with high contrast, but part B of the test chart is invisible. When part B is thicker, the light pulse takes a longer time to pass through part B, which will be time-gated out at the time $t = 0$ ps. Further, we can obtain the image of part B of the test chart by adjusting the delay time between the gating pulse and the imaging pulse. The corresponding image is shown in Fig.4(c) at the time $t = 2$ ps. This result implies that the DOKG microscopic imaging technique can be used to obtain the image of different parts of inhomogeneous objects hidden in turbid media.

IV. CONCLUSIONS

In summary, we have demonstrated a new method for microscopy imaging through a turbid medium by use of a DOKG. Subtracting the positive heterodyne OKG microscopic image from the negative heterodyne OKG microscopic image, we obtain the DOKG microscopic image. The results show that the background light can be removed and the high spatial frequency components of the imaged object filtered by the optical Kerr gate can be considerably compensated by use of a DOKG. The contrast of microscopy images obtained by using the DOKG technique can be enhanced significantly compared with OKG microscopic imaging. The present work is mainly devoted to the study of the spatial resolution of the DOKG microscopic imaging. The images of the test chart (a U.S. Air Force 1951 resolution chart) hidden behind a polystyrene microsphere sample are demonstrated by use of DOKG microscopic imaging. The DOKG microscopic imaging technique is potentially applicable to obtain the images of the structure in a real spray.

REFERENCES

[1] E. P. Zege, L. L. Katsev, and I. N. Polonsky, "Multicomponent approach to light propagation in clouds and mists," *Appl. Opt.*, vol. 32, no. 15, pp. 2803–2812, 1993.

[2] R. N. Mahalati and J. M. Kahn, "Effect of fog on free-space optical links employing imaging receivers," *Opt. Exp.*, vol. 20, no. 2, pp. 1649–1661, 2012.

[3] S. Idlahcen, C. Rozé, L. Méès, T. Girasole, and J.-B. Blaisot, "Sub-picosecond ballistic imaging of a liquid jet," *Experim. Fluids*, vol. 52, no. 2, pp. 289–298, 2012.

[4] B. B. Das, K. M. Yoo, and R. R. Alfano, "Ultrafast time-gated imaging in thick tissues: A step toward optical mammography," *Opt. Lett.*, vol. 18, no. 13, pp. 1092–1094, 1993.

[5] K. M. Yoo, F. Liu, and R. R. Alfano, "Imaging through a scattering wall using absorption," *Opt. Lett.*, vol. 16, no. 14, pp. 1068–1070, 1991.

[6] L. Wang, P. P. Ho, C. Liu, G. Zhang, and R. R. Alfano, "Ballistic 2-D imaging through scattering walls using an ultrafast optical Kerr gate," *Science*, vol. 253, no. 5021, pp. 769–771, 1991.

[7] W. Chu *et al.*, "Lasing action induced by femtosecond laser filamentation in ethanol flame for combustion diagnosis," *Appl. Phys. Lett.*, vol. 104, no. 9, p. 091106, 2014.

[8] H.-L. Li, H.-L. Xu, B.-S. Yang, Q.-D. Chen, T. Zhang, and H.-B. Sun, "Sensing combustion intermediates by femtosecond filament excitation," *Opt. Lett.*, vol. 38, no. 8, pp. 1250–1252, 2013.

[9] H. L. Xu and S. L. Chin, "Femtosecond laser filamentation for atmospheric sensing," *Sensors*, vol. 11, no. 1, pp. 32–53, 2011.

[10] W. Tan *et al.*, "High contrast ballistic imaging using femtosecond optical Kerr gate of tellurite glass," *Opt. Exp.*, vol. 21, no. 6, pp. 7740–7747, 2013.

[11] A. D. Sappey, "Optical imaging through turbid media with a degenerate four wave mixing correlation time gate," *Appl. Opt.*, vol. 33, no. 36, pp. 8346–8354, 1994.

[12] R. Ambekar, T.-Y. Lau, M. Walsh, R. Bhargava, and K. C. Toussaint, Jr., "Quantifying collagen structure in breast biopsies using second-harmonic generation imaging," *Biomed. Opt. Exp.*, vol. 3, no. 9, pp. 2021–2035, 2012.

[13] L. Wang, P. P. Ho, and R. R. Alfano, "Time-resolved Fourier spectrum and imaging in highly scattering media," *Appl. Opt.*, vol. 32, no. 26, pp. 5043–5048, 1993.

[14] B. L. Yu, A. B. Bykov, T. Qiu, P. P. Ho, R. R. Alfano, and N. Borreli, "Femtosecond optical Kerr shutter using lead–bismuth–gallium oxide glass," *Opt. Commun.*, vol. 215, pp. 407–411, Jan. 2003.

[15] F. Mathieu, M. A. Reddemann, J. Palmer, and R. Kneer, "Time-gated ballistic imaging using a large aperture switching beam," *Opt. Exp.*, vol. 22, no. 6, pp. 7058–7074, 2014.

[16] M. Seo *et al.*, "Ultrafast optical wide field microscopy," *Opt. Exp.*, vol. 21, no. 7, pp. 8763–8772, 2013.

[17] X. Gan, S. Schilders, and M. Gu, "Combination of annular aperture and polarization gating methods for efficient microscopic imaging through a turbid medium: Theoretical analysis," *Microscopy Microanal.*, vol. 3, no. 6, pp. 495–503, 1997.

[18] I. Grulkowski *et al.*, "High-precision, high-accuracy ultralong-range swept-source optical coherence tomography using vertical cavity surface emitting laser light source," *Opt. Lett.*, vol. 38, no. 5, pp. 673–675, 2013.

[19] S. P. Chong, C. H. Wong, K. F. Wong, C. J. R. Sheppard, and N. Chen, "High-speed focal modulation microscopy using acousto-optical modulators," *Biomed. Opt. Exp.*, vol. 1, no. 3, pp. 1026–1037, 2010.

[20] P. Guitera *et al.*, "The impact of *in vivo* reflectance confocal microscopy on the diagnostic accuracy of lentigo maligna and equivocal pigmented and nonpigmented macules of the face," *J. Invest. Dermatol.*, vol. 130, no. 8, pp. 2080–2091, 2010.

[21] D. Sedarsky, J. Gord, C. Carter, T. Meyer, and M. Linne, "Fast-framing ballistic imaging of velocity in an aerated spray," *Opt. Lett.*, vol. 34, no. 18, pp. 2748–2750, 2009.

[22] X. Liang, L. Wang, P. P. Ho, and R. R. Alfano, "Two-dimensional Kerr–Fourier imaging of translucent phantoms in thick turbid media," *Appl. Opt.*, vol. 34, no. 18, pp. 3463–3467, 1995.

[23] M. E. Orczyk, M. Samoc, J. Swiatkiewicz, and P. N. Prasad, "Dynamics of third-order nonlinearity of canthaxanthin carotenoid by the optically heterodyned phase-tuned femtosecond optical Kerr gate," *J. Chem. Phys.*, vol. 98, no. 4, pp. 2524–2533, 1993.

[24] Q. Zhong and J. T. Fourkas, "Optical Kerr effect spectroscopy of simple liquids," *J. Phys. Chem. B*, vol. 112, no. 49, pp. 15529–15539, 2008.

[25] W. Tan *et al.*, "Sharpness-enhanced ultrafast imaging by using a biased optical Kerr gate," *Opt. Exp.*, vol. 22, no. 23, pp. 28100–28108, 2014.